Monthly Notices
of the
ROYAL ASTRONOMICAL SOCIETY

Mon. Not. R. Astron. Soc. **415,** 1051–1060 (2011) doi:10.1111/j.1365-2966.2011.18545.x

Hierarchical formation of bulgeless galaxies: why outflows have low angular momentum

C. B. Brook,[1⋆] F. Governato,[2] R. Roškar,[2,3] G. Stinson,[1] A. M. Brooks,[4] J. Wadsley,[5] T. Quinn,[2] B. K. Gibson,[1] O. Snaith,[1] K. Pilkington,[1] E. House[1] and A. Pontzen[6]

[1] *University of Central Lancashire, Jeremiah Horrocks Institute for Astrophyics & Supercomputing, Preston PR1 2HE*
[2] *Astronomy Department, University of Washington, Box 351580, Seattle, WA 98195-1580, USA*
[3] *Institute for Theoretical Physics, University of Zürich, Winterthurerstrasse 190, Zürich, Switzerland*
[4] *California Institute of Technology, M/C 130-33, Pasadena, CA 91125, USA*
[5] *Department of Physics and Astronomy, McMaster University, Hamilton, ON L8S 4M1, Canada*
[6] *Institute of Astronomy and Kavli Institute for Cosmology Cambridge, Madingley Road, Cambridge CB3 0HA*

Accepted 2011 February 15. Received 2011 January 24; in original form 2010 September 29

ABSTRACT

Using high resolution, fully cosmological smoothed particle hydrodynamical simulations of dwarf galaxies in a Lambda cold dark matter Universe, we show how high redshift gas outflows can modify the baryon angular momentum distribution and allow pure disc galaxies to form. We outline how galactic outflows preferentially remove low angular momentum material due a combination of (a) star formation peaking at high redshift in shallow dark matter potentials, an epoch when accreted gas has relatively low angular momentum, (b) the existence of an extended reservoir of high angular momentum gas in the outer disc to provide material for prolonged SF at later times and (c) the tendency for outflows to follow the path of least resistance which is perpendicular to the disc. We also show that outflows are enhanced during mergers, thus expelling much of the gas which has lost its angular momentum during these events, and preventing the formation of 'classical', merger driven bulges in low-mass systems. Stars formed prior to such mergers form a diffuse, extended stellar halo component similar to those detected in nearby dwarfs.

Key words: galaxies: bulges – galaxies: evolution – galaxies: formation – galaxies: starburst.

1 INTRODUCTION

The angular momentum of disc galaxies is thought to originate from tidal torques imparted by surrounding structures in the expanding Universe (Peebles 1969; Barnes & Efstathiou 1987), prior to protogalactic collapse. Disc galaxies will form if we assume that gas gains the same amount of angular momentum as the dark matter in this process, and that this angular momentum is retained as the gas cools to the centres of dark matter haloes (Fall & Efstathiou 1980). Gas subsequently fragments and forms stars. Within cold dark matter (CDM) cosmology this picture of the origin of galactic angular momentum is believed to hold even as galaxies are built hierarchically, with the added assumption that mergers result in building bulge components (Barnes & Hernquist 1996).

However, detailed modelling has highlighted problems with this scenario. In simulations, gas cools to the centre of the earliest collapsing structures making them very centrally concentrated. Dynamical friction occurring during the mergers of such systems results in significant loss of angular momentum (Navarro & Steinmetz 2000; Maller & Dekel 2002). This problem has largely been overcome in simulations by increasingly effective recipes for feedback from supernovae (Thacker & Couchman 2000; Stinson et al. 2006; Governato et al. 2007), and increased resolution (Sales et al. 2010). Despite this encouraging progress, decreasing the impact of dynamic friction does not solve all the problems of galaxy formation which relate to angular momentum within hierarchical structure formation (Mayer, Governato & Kaufmann 2008). Simulations continue to produce centrally concentrated systems, resulting in 'peaked' rotation curves which do not match those of observed galaxies (Governato, Mayer & Brook 2008; Dutton & van den Bosch 2009). In addition, the angular momentum distribution of baryons in real galaxies differs significantly from the distribution within dark matter haloes (van den Bosch, Burkert & Swaters 2001). Even if angular momentum were fully conserved, CDM haloes have a low angular momentum tail (Navarro, Frenk & White 1996; Bullock et al. 2001). Recent simulations show that galaxies formed in a CDM Universe have realistic disc sizes (Brooks et al. 2010), however the coupling of dark matter and gas while acquiring their

⋆E-mail: cbabrook@gmail.com

angular momentum thus implies that baryons should also have such a low angular momentum component, which is generally believed to be reflected in bulge components (van den Bosch 2001). Yet many low-mass galaxies have no bulge; ∼70 per cent of galaxies with stellar mass of $<10^9\,M_\odot$ have a Sersic index of less than 1.5 (Dutton 2009) and many more massive galaxies do not have classical bulges (Kormendy et al. 2010; Fisher & Drory 2010). Pure disc structures reflect an underlying angular momentum distribution which is seemingly at odds with theories of galaxy formation within the accepted ΛCDM paradigm (Bullock et al. 2001; van den Bosch 2001). The only way to reconcile ΛCDM with observations of bulgeless disc galaxies is to alter the distribution for the baryons, or to remove the low angular momentum tail. In a hierarchical ΛCDM Universe, mergers also drive gas towards inner regions, forming low angular momentum bulge stars. The persistence and degree of these problems means that the manner in which disc galaxies attain and retain their angular momentum has continued to be considered one of the major challenges to the ΛCDM paradigm.

The removal of gas in galactic outflows is one avenue worth exploring in order to explain the discrepancy in angular momentum distributions between dark matter and baryons (Binney, Gerhard & Silk 2001). Several lines of evidence suggest that supernova driven galactic winds are able to expel large amounts of gas from galaxies during the galaxy formation process (Mathews & Baker 1971; Veilleux, Cecil & Bland-Hawthorn 2005). Galactic winds have been observed, and extensively studied in local star-forming galaxies (e.g. Lynds & Sandage 1963; Axon & Taylor 1978; Martin 1999; Ohyama 2002; Martin, Fanson & Schiminovich 2005; Rupke, Veilleux & Sanders 2005). Outflows are expected to be more common at high redshift where star formation is more active (Madau et al. 1996). Indeed, outflows have been detected at high redshift from Lyman-break selected galaxies (Pettini et al. 1998; Simcoe, Sargent & Rauch 2002; Shapley et al. 2003; Adelberger et al. 2005), as well as gravitationally lensed galaxies (Pettini et al. 2000).

We recently simulated dwarf galaxies which match a wide range of observed dwarf galaxy properties, including the absence of a bulge, and a linearly rising rotation curve with no inner 'peak' which characterizes previous simulations (Governato et al. 2010; G10 hereafter). The simulated galaxies lie on the Tully–Fisher relation, and the size–luminosity relation (Brooks et al. 2011). Using techniques which closely mimic observations, the galaxies have been shown to have mass distributions which are consistent with galaxies in the THINGS Survey (Oh et al. 2011), and fall on the baryonic Tully–Fisher relation, as derived by McGaugh (2005). Most importantly, the simulated dwarfs also match the distribution of angular momentum of stars observed in pure disc galaxies, differing significantly from that of the dark matter halo in which they are embedded (see fig. 4 of G10, as well as Fig. 8 of this paper). These properties indicate that our simulations can provide unique insights into the acquisition and retention of angular momentum of disc galaxies. Here we provide an overview of the various interlinked processes which determine the angular momentum distribution of stars in our simulated bulgeless disc galaxy. In particular we outline why the significant amount of gas which is expelled from the galaxy is primarily low angular momentum material.

In Section 2, we review the code and the simulation initial conditions. We present the properties of our simulated galaxy in Section 2.1. We plot star formation rates and outflow rates, as well as their ratio (the 'mass loading') in Section 3. We show that the outflows have a strong bias towards low angular momentum in Section 4. We outline the reasons for outflows having preferentially low angular momentum material: early accreted material has low angular momentum, yet needs to escape a relatively low potential well (Section 4.1); the existence of an extended reservoir of high angular momentum gas (Section 4.2); with outflows being perpendicular to the disc (Section 4.3). We also show that the starburst triggered in the late merger expels the bulk of the gas which lost its angular momentum during this event (Section 4.4). Our summary and discussion follows in Section 5.

2 THE SIMULATION

At $z = 0$ the virial mass of the halo in the dark matter only run of our simulated galaxy is $4.8 \times 10^{10}\,M_\odot$ (the virial mass is measured within the virial radius R_{vir}, the radius enclosing an overdensity of 100 times the cosmological critical density). The halo was selected within a large scale, low resolution, simulation run in a concordance, flat, Λ-dominated cosmology: $\Omega_0 = 0.24$, $\Lambda = 0.76$, $h = 0.73$, $\sigma_8 = 0.77$ and $\Omega_b = 0.042$ (Spergel et al. 2003; Verde et al. 2003).

We evolved the simulation using the fully parallel, *N*-body+smoothed particle hydrodynamics (SPH) code GASOLINE which self-consistently models gas hydrodynamics and cooling, star formation and energy feedback from supernovae, with structure formation driven by the hierarchical growth of CDM. A detailed description of the code is available in the literature (Wadsley, Stadel & Quinn 2004). The version of the code used in this study includes radiative cooling and accounts for the effect of a uniform background radiation field on the ionization and excitation state of the gas. The cosmic ultraviolet background is implemented using the Haardt–Madau model (Haardt & Madau 1996); we use a standard cooling function for a primordial mixture of atomic hydrogen and helium at high gas temperatures, but we include the effect of metal cooling for $T < 10^4$ (Bromm et al. 2001; Mashchenko et al. 2008). The possible effects of including H_2 metal line cooling and SF linked to H2 abundance and some preliminary results are briefly discussed in Section 5.

Star formation occurs when cold gas reaches a given threshold density (Stinson et al. 2006), which is dependent on the volume of the star-forming regions that can be resolved (Robertson & Kravtsov 2008; Saitoh et al. 2008; Tasker & Bryan 2008). We used 100 amu cm^{-3} in the main run analysed here. The adoption of a higher density threshold for star formation (most previous studies used 0.1 amu cm^{-3}) has the effect of limiting SF to gas clumps similar in mass to real star forming regions and increasing drastically the amount of energy per unit mass released into the gas directly affected by supernova feedback. This higher threshold is justified by the high mass and spatial resolution of this run that allow individual star-forming regions to be resolved. Star formation then proceeds at a rate proportional to $\rho_{gas}^{1.5}$, i.e. locally enforcing a Schmidt law. The adopted feedback scheme is implemented by releasing thermal energy from supernovae into the gas surrounding each star particle (Stinson et al. 2006). The energy release rate is tied to the time of formation of each particle (which effectively ages as a single stellar population with a Kroupa IMF). To model the effect of feedback at unresolved scales, the affected gas has its cooling shut off for a time-scale proportional to the Sedov solution of the blastwave equation, which is set by the local density and temperature of the gas and the amount of energy involved. In the central run described in this study this translates into regions of ∼150 to 400 pc in radius being heated by feedback from multiple, overlapping supernovae, and having their cooling shut off for typically 5–10 Myr. However, even during high-z starbursts only a few per cent of the gas in the disc plane is heated by supernova feedback to temperatures >40 000 K. The effect of feedback is to regulate star formation efficiency as a

function of mass (Brooks et al. 2007). Only two other parametres are needed, the star formation efficiency (ϵSF = 0.1) and the fraction of supernova energy coupled to the inter stellar medium (ISM) (eSN = 0.4). Similar values have been used in previous works by this group (Governato et al. 2007). However, here we slightly increased ϵSF from 0.05 to 0.1 to ensure a better normalization to the local Schmidt law. We explored values of eSN as high as 0.6 and cooling shut-off times changing by a factor of a few to verify that results are robust to small changes in the description of SF.

2.1 The galaxy: resolution and cosmic variance

The simulation presented here is part of an ongoing campaign to study the formation and evolution of galaxies in a ΛCDM cosmology. Recent work has highlighted the role of numerical resolution in driving the structural properties of simulated galaxies and specifically their internal mass distribution (Mayer et al. 2008). We analysed the simulated galaxy used in this study at different resolutions and showed that our key results are retained at high resolution regimes, which have spatial resolution less than ∼200 pc and gas particle mass less than a few $10^4\,M_\odot$ (G10). Yet we emphasize the importance of resolving star-forming regions by allowing gas to collapse to high-density regions during these merger events. For example a high SF threshold DG1MR forms about $3\times10^8\,M_\odot$ in stars. This relatively low star formation efficiency leads to an $M_{\rm stars}/M_{\rm halo}$ ratio of 1/200, which is close to what is measured for nearby small galaxies with resolved kinematics and photometry (Oh et al. 2010). On the other hand, a 0.1 amu/cm^3 threshold allows eight times more stars to form (see G10, online material). Adopting high resolution significantly decreases SF also in halos with mass $>10^{11}\,M_\odot$ (Governato et al., in preparation; Mayer et al., in preparation), reducing the overproduction of stars (Brooks et al. 2010) and bringing them close to estimates for more massive galaxies (Guo et al. 2010) that predict $M_{\rm stars}/M_{\rm halo}\sim0.04-0.05$.

To closely study outflows, we generated frequent outputs in order to determine outflow rates and the properties of the gas prior to being blown out. To this end, we use DG1MR from G10, which has outputs every ∼500 Myr, and has an effective resolution 2048^3 in a 25-Mpc box, with gravitation softening of 110 pc and typical stellar mass of $\sim1700\,M_\odot$. The morphology (that of a bulgeless dwarf irregular galaxy), star formation rate, final stellar and baryon fraction, $M_{\rm H\,I}/L_{\rm B}$, rotation velocity, magnitude and colour show little change between DG1 and DG1MR. These properties contrast significantly compared to the same simulation run with a low threshold for star formation (DG1LT), which does not generate large scale outflows. Details of the properties of the galaxies DG1, DG1MR and DG1LT using techniques which mimic observations were presented in G10. DG1MR has $M_i=-16.9$, $g-r=0.54$, $M_{\rm star}=5.3\times10^8\,M_\odot$, scalelength $R_{\rm s}=0.9$ kpc, rotational velocity $V_{\rm rot}=55\,{\rm km\,s^{-1}}$ and ratio of neutral hydrogen to B-band luminosity $M_{\rm H\,I}/L_{\rm B}=1.0$.

Bulges are commonly asserted to be formed in mergers, with galaxies which have more mergers, or mergers with larger mass ratios, assumed to have larger bulges (e.g. Hopkins et al. 2010). Merger histories of low-mass galaxies are equally as diverse and rich as high-mass galaxies, yet it is only in low-mass galaxies where bulgeless discs are common (Dutton 2009). Simulations should be able to form low-mass galaxies with low B/D ratios and rising rotation curves starting from different realizations of cosmological initial conditions. It is important to highlight that the success of our analysed galaxy is not a result of a particular, special merging history. We showed in G10 the results of two simulations which had very different merging histories, highlighting that we have not selected a particularly quiescent simulated galaxy. In Fig. 1, we plot a type of merger tree for the simulation analysed in this study, which shows the birth position within the simulation box of every star which ends up in the final galaxy at $z=0$. We are tracing the birth of stars as the galaxy falls through the simulation box. The axes are the x and y coordinates of the simulation box, shown in comoving kpc. The colours are the birth time of stars. We see in this plot the merger events which involve satellites which are large enough to host stars. Two significant merger events in particular can be seen at ∼2.5 and ∼7 Gyr. Prior to merging, Sat1 has a virial mass of $1.4e9\,M_\odot$, gas mass of $2.0e8\,M_\odot$ and stellar mass of $3.7e6\,M_\odot$, with the central galaxy having virial mass of $4.6e9\,M_\odot$, gas mass of $2.6e8\,M_\odot$ and stellar mass of $4.1e7\,M_\odot$ at a corresponding time. Also evident are the passages of Sat2 around the central galaxy and hence its merging period which extends for ∼1.6 Gyr between ∼5.2 Gyr ($z=1.2$) and final coalescence at ∼6.8 Gyr ($z=0.8$). Prior to merging, Sat2 has a virial mass of $4.9e9\,M_\odot$, gas mass of $3.4e8\,M_\odot$ and stellar mass of $3.8e7\,M_\odot$, while the central galaxy has virial mass of $1.4e10\,M_\odot$, gas mass of $1.3e9\,M_\odot$ and stellar mass of $1.8e8\,M_\odot$ at a corresponding time.

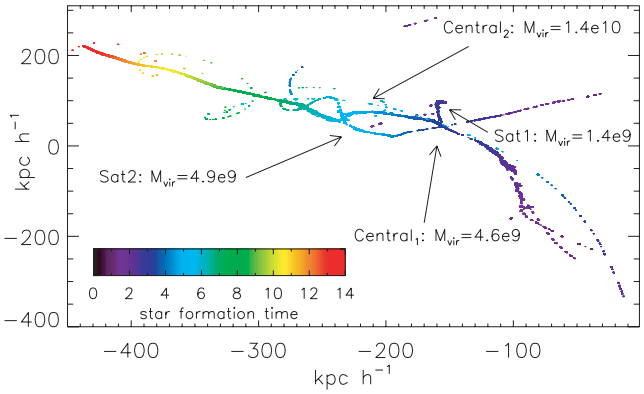

Figure 1. A type of merger tree. We plot the birth position within the simulation box of every star which ends up in the final galaxy at $z=0$. We are tracing the birth of stars as the galaxy moves through the simulation box. The axis are the x and y coordinates of the simulation box, shown in comoving kpc. The colours are the birth time of the stars, where $z=0$ corresponds to 13.7 Gyr. We see in this plot the merger events which involve satellites which are large enough to host stars. Two significant merger events in particular can be seen at ∼2.5 and ∼7 Gyr. For these events, we note the virial mass of the satellites (Sat1 and Sat2) prior to the merger, as well as the mass of the central galaxy at corresponding times. The passages of Sat2 around the central galaxy and its extended merging period is also evident.

3 STAR FORMATION AND OUTFLOWS

Fig. 2 shows the star formation rate as a function of time for our simulated galaxy. In red, we show the star formation using 200-Myr bins. The bursty nature of star formation is apparent. The black line shows 1-Gyr bins, to allow a better match to the time resolution we have for our outflows in subsequent plots. Star formation shows bursts, some of which are associated with mergers, with a high star formation rate at ∼2.5 Gyr associated with Sat1, and then peaks again at ∼7 Gyr. This final increase in the star formation rate is associated with the last major merger (Sat2), which has a mass ratio of ∼3:1. Subsequent to the end of this merger, the star formation rate decreases significantly, and is quite low for the final ∼4 Gyr but continues to be bursty.

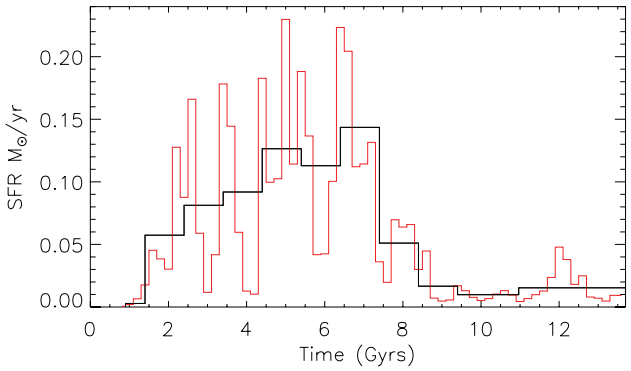

Figure 2. The star formation rate plotted as a function of time. We show 200-Myr bins in red, highlighting the bursty nature of the star formation. The black line shows 1-Gyr bins, which is shown because that matches the time resolution information that we have for outflows, which are less well defined than star formation. The peak in star formation at ∼7 Gyr is associated with the last major merger.

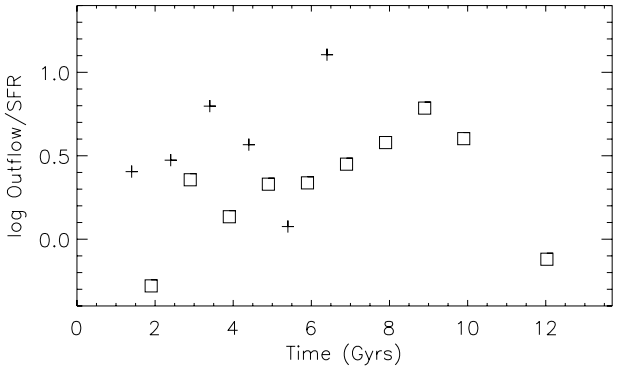

Figure 4. The evolution of the ratio of the mass of expelled gas to the mass of stars formed, showing a 'mass loading' from the central galaxy (square symbols) of greater than one for almost the entire simulation, and a rise associated with a late major merger event. The crosses show the mass loading of the major satellite which merges at $z \sim 1$, which also shows significant outflows.

The outflow rate, in $M_\odot$ yr^{-1}, is shown in Fig. 3. The black line shows the outflows from the central galaxy. The red dashed line adds outflows from the two most significant satellites accreted during the galaxy's evolution, marked Sat1 and Sat2 in Fig. 1. Outflows are calculated in a very simple manner; any gas which is bound and within $5R_*$ at any output time-step, but is outside $R_{\rm vir}$ of the final galaxy at $z = 0$, is assumed to have been expelled, where R_* is the radial distance to the furthest star from the centre of the galaxy. Typically, R_* is $\sim 0.5\,R_{\rm vir}$. Our results are not sensitive to this choice, so long as the radius is well beyond the star-forming region which means that we do not miss gas which is being expelled, and is not too close to $R_{\rm vir}$, which can result in gas which is not bound being falsely identified as outflows. We only include gas which does not return to the galaxy at later times in our definition of outflows in this study. Using 28 outputs which are ∼500 Myr apart, each outflow particle is traced through every output to find the maximum 'jump' in radial distance from the centre. The jump in radius is invariably associated with a temperature that shows that the gas particle was heated by supernova energy. The time of the radial and temperature jump determines the outflow time for the particle.

We note that the degree and direction of outflows in our simulation are not put in our code by hand as is common in kinetic feedback schemes (e.g. Navarro & Steinmetz 2000; Springel & Hernquist 2003; Oppenheimer & Davé 2006), but occur naturally due to thermal pressure exerted on gas in our formulation of supernova feedback.

The general shape of the outflows histogram is similar to the star formation rate, including a particularly prominent peak in outflows during the coalescence of the last major merger event at time ∼7 Gyr ($z \sim 0.8$). This correspondence between a merger induced starburst and subsequent outflows is discussed in Section 4.4.

The ratio of the outflows from the central galaxy to the star formation rate is called the 'mass loading' or the 'loading factor'. The log of the ratio of the outflows from the central galaxy to the star formation rate is shown in Fig. 4 (squares). The mean mass loading from the central galaxy throughout the simulated galaxy's evolution is 2.3, with a significant increase associated with the merger at ∼7 Gyr. We will see that a high mass loading is a crucial ingredient that determines the final angular momentum content of our simulated galaxy. In Fig. 4 we also show the mass loading of the outflows from the major satellite, Sat2 (crosses), which merges to the central galaxy at $z \sim 1$. This highlights that outflows also occur from the satellites which are massive enough to from stars. From here on, we analyse properties of outflows from the central galaxy, or main progenitor, at each time and simply refer to 'outflows'.

In Fig. 5 we plot the cumulative mass of such identified outflows as a function of circular velocity at the time of expulsion. It is

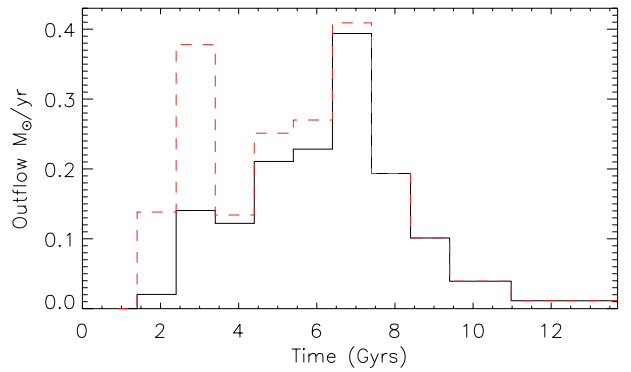

Figure 3. The outflow rate of gas from the galaxy as a function of time. The black line shows the outflows from the central galaxy. The red dashed line adds outflows from the two most significant satellites accreted during the galaxy's evolution. The peak outflows occur during the merger events at ∼2.5 and ∼7 Gyr.

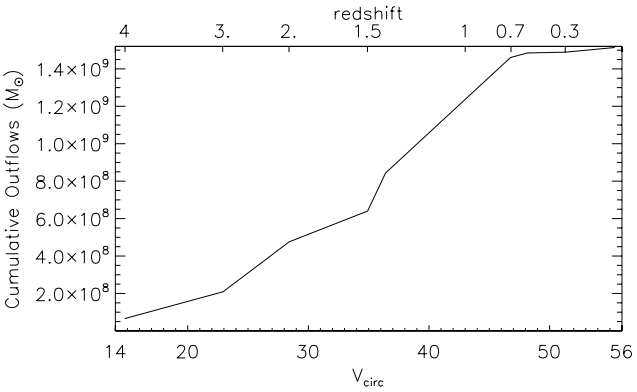

Figure 5. The cumulative mass of outflows as a function of circular velocity. Significant outflows occur prior to the simulated galaxy attaining all its material. The top axis indicates the corresponding redshifts.

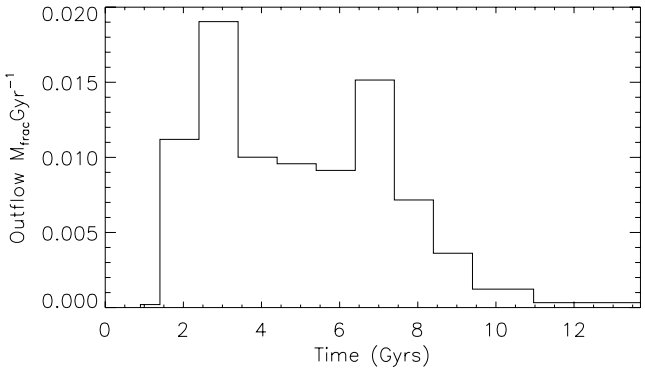

Figure 6. The evolution of the ratio of the mass of expelled gas to the total virial mass of the galaxy. The ratio peaks at early times, with the subsequent steady decline interrupted by a rise which occurs during the last major merger event.

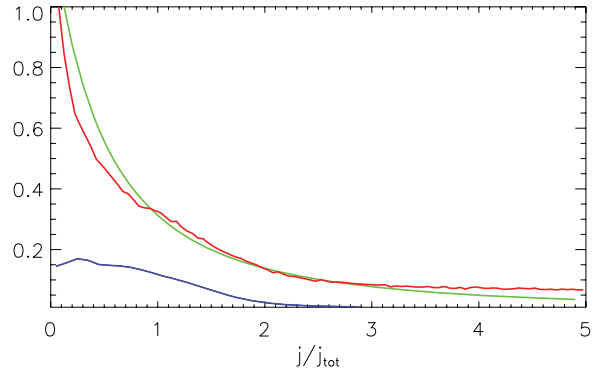

Figure 8. The final distribution of $j = rV_c(r)$ for 'observable' baryons in the simulation, which consists of stars and H I gas (blue). In red we plot the distribution of all baryons which would have ended in the galaxy if outflows were not present, i.e. it is the distribution of stars, H I gas and warm/hot gas within the virial radius at $z = 0$, combined with outflows whose angular momentum is determined at the time-step prior to being heated and expelled. An analytic fit, as determined in Bullock et al. (2001), to the typical distribution for dark matter haloes is overplotted (green).

apparent that significant amounts of material are expelled while the galaxy is still relatively low mass, but that the galaxy continues to accrete material and grow. The early expulsion is particularly significant relative to the low mass of the galaxy at those times, and this has the effect of altering the final angular momentum distribution of the baryons. To highlight this, we plot the evolution of the ratio of outflows to the total mass of the galaxy (M_{frac}) in Fig. 6. This plot shows a peak in the fraction of mass being ejected at early times, between 2 and 3 Gyr, when the potential of the protogalaxy is relatively low and the outflow rate is high. A subsequent steady decline in M_{frac} is halted only during the last merger at ∼7 Gyr, during which large outflows occur.

4 SELECTIVE REMOVAL OF LOW ANGULAR MOMENTUM IN OUTFLOWS

As a consequence of the strong outflows 70 per cent of the baryons are expelled by winds during the galaxy's evolution, and there is a significant bias toward low angular momentum in the expelled gas. Fig. 7 compares the j_z distribution of gas which has been ejected in outflows (black line) to the j_z distribution of all baryons within the virial radius of the galaxy at $z = 0$, showing gas (red), H I gas (red dashed) and stars (blue). Here, j_z is the component of the angular momentum whose vector is perpendicular to the disc. The angular momentum of the outflowing material is determined

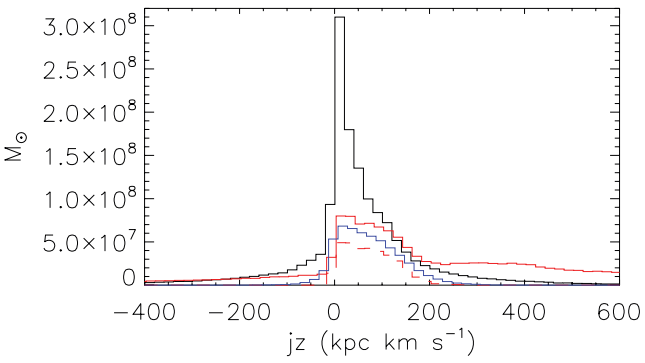

Figure 7. The angular momentum distributions of stars (blue), all gas (red) and H I gas (red dashed) within the virial radius at $z = 0$ and gas which is blown out of the galaxy throughout its evolution (black). A bias for low angular momentum to be expelled is evident, as is the fact that a large amount of material is expelled.

at the time-step prior to its heating and ejection from the central galaxy. The shape of the angular momentum distribution of the ejected material differs strongly from the material which makes up the galaxy at $z = 0$. The outflow comprises a large low angular momentum peak. The outflows also display a significant tail of negative angular momentum material. By contrast, the warm/hot gas in the galaxy at $z = 0$ contains high angular momentum material, while the cold (HI) gas and stars have very little negative angular momentum material and relatively little low angular momentum material. We note that a very similar result occurs when total angular momentum is plotted, which we omit for brevity.

In order to make a more direct link to observations, Fig. 8 shows the angular momentum distribution, j/j_{tot}, for 'observable' baryons, defined as a combination of stars and cold (HI) gas in order to mimic van den Bosch et al. (2001), who plot such a distribution for several observed galaxies. Here, j_{tot} is the mean angular momentum of these 'observable' baryons, and the angular momentum is derived using $j = rV_c(r)$, where r is the radius and V_c the circular velocity. We also plot the distribution of all baryons as they would be in the absence of outflows (red line). That is to say, the distribution of outflows, as measured just prior to the time of ejection, plus all baryons within the virial radius at $z = 0$. This distribution is also normalized by the same j_{tot} of the disc baryons, in order to allow direct comparison with the blue line which represents the distribution of observable baryons. A very different distribution is apparent between what is observed at $z = 0$, and the total baryonic component in absence of outflows. In particular a large amount of low angular momentum gas is present due to the expelled low angular momentum gas, as well as a high angular momentum tail of warm/hot gas.

Also shown on this plot is the distribution of angular momentum, normalized by the mean angular momentum, for a typical dark matter halo, as characterized in Bullock et al. (2001) and used in van den Bosch et al. (2001). The total baryons which would have been in the galaxy in the absence of outflows (red line) have a very similar shape to this distribution, although we note that the normalization, j_{tot}, that we used was the mean angular momentum of the disc baryons. Normalizing by the mean of the total angular momentum of baryons which would have been in the galaxy at $z = 0$ would shift the distribution to the left. Nevertheless, the shape

of the distribution of all baryons which would have been in the galaxy in the absence of outflows, and that of dark matter haloes, are remarkably similar, highlighting the role that outflows play in causing the distribution of observed baryons to differ so sharply from their host haloes.

We now identify the processes which result in the strong bias towards low angular momentum of outflows that we have identified. Although identified separately, these processes are interlinked. In combination they result in the ejection of low angular momentum material and a significant alteration of the angular distribution of baryons, and in particular the distribution of stars and cold (HI) gas within galaxies compared to their host dark matter haloes.

4.1 Early accreted material has low angular momentum

Material which falls into the central regions of protogalaxies at the earliest times has been subjected to the least amount of torquing from the large scale structure (Ryden 1988; Quinn & Binney 1992). Material falling in at later times has higher angular momentum. This results in early outflows having less angular momentum than later outflows, and introduces a bias whereby low angular momentum material is expelled. Fig. 9 shows the evolution of j_z of outflows (squares), calculated at the time of ejection, as well as the inflows (blue line) at a corresponding time. Also shown is the evolution of j_z for the baryons (red line) and dark matter (green line) which end up in the galaxy at $z = 0$. A similar plot results when total angular momentum is plotted in this manner. The central galaxy, or main progenitor, is used as a reference frame at all times, and as we stated above, outflows are those ejected from the central galaxy, while inflows, described below, are also to the central galaxy.

After spinning up, the dark matter material which ends in the galaxy at $z = 0$ essentially retains its angular momentum. The baryons which end up in the galaxy at $z = 0$ have also retained their angular momentum. At the early times, it is low angular momentum material that has been accreted and is hence available for blow out and this is reflected in the very low angular momentum of material which is ejected at early times. Only gas which has been accreted can be ejected, so a large bias is clear between ejected gas and the gas which will end up in the galaxy at $z = 0$. Thus, in the absence of this gas turning into stars and hence being 'set' with this low angular momentum, there is a simple bias for early, low angular momentum gas to be blown out over later accreted, higher angular momentum gas. The low star formation rates and relatively high blowout rates (i.e. the high mass loading, see Fig. 4) means that a large fraction of low angular momentum material is not forming stars. As outer, high angular momentum shells of gas are accreted, they make up a larger fraction of the angular momentum distribution of gas than they would if none of the earlier accreted gas were expelled. This naturally alters the distribution of gas *angular momentum* compared with dark matter. Low star formation efficiency and high gas fractions mean that *blown out gas* has preferentially *low angular momentum*.

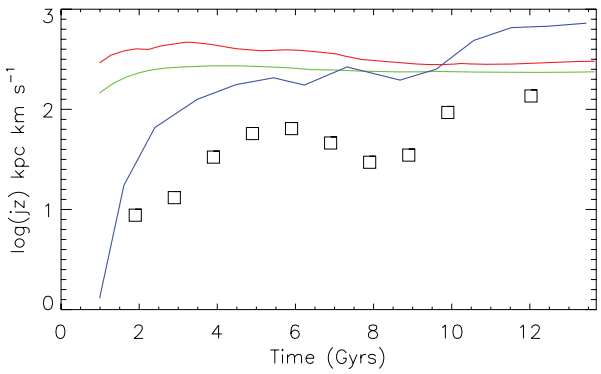

Figure 9. The evolution of the mean angular momentum (j_z) of baryons (red) and dark matter (green) which are within the virial radius at $z = 0$, compared with the mean angular momentum of gas which is being ejected during the galaxy's evolution (squares). Also shown is the mean angular momentum of gas which is being accreted at each time (blue line). Material which collapses early into the galaxy has relatively low angular momentum, and is available for being expelled, and this is replaced by inflowing gas which has progressively higher angular momentum.

The blue line traces the angular momentum of inflowing gas at each time. We define inflowing material as gas which has reached $5R_*$ for the first time, in order to make a fair comparison with the outflowing material as we have defined it (recall that R_* is the radial distance to the furthest star from the centre of the galaxy at each time). Clearly, inflowing gas has significantly higher angular momentum than the outflows at all times. At late times, the inflowing material has higher angular momentum than the mean of all gas which is within the virial radius at $z = 0$, reflecting the fact that later accreted material has high angular momentum.

Lower potential wells at early times favour higher blowout rates, as a function of galactic mass, at a time when lower angular momentum material is being accreted.

4.2 Extended reservoir of high angular momentum material

Star formation only occurs in the inner regions of the galaxy where the gas reaches sufficiently high densities. Extended H I gas discs are found around local isolated low mass galaxies (Broeils & Rhee 1997). Such low mass, isolated galaxies have gas dominating their baryonic mass fractions, with values typically above 70 per cent, and as high as 95 per cent (Schombert, McGaugh & Eder 2001; Geha et al. 2006) There is evidence that extended H I discs occur in intermediate (Puech et al. 2010) and high redshift galaxies (Daddi et al. 2010). Further, there is evidence for the existence of warm/hot gas in the haloes of disc galaxies (Spitzer 1956; Spitzer & Jenkins 1975; Sembach et al. 2003). In our simulations, gas beyond the star formation region serves as a repository of high angular momentum material. Typically, between 30 and 40 per cent of gas within the virial radius of our simulated galaxy lies within the star-forming region at a given time. Fig. 10 shows the face-on *B*-band surface brightness map of the galaxy at $z \sim 1.2$, over plotted by an H I contour map. The extent of the star-forming region, from which outflows are driven, is reflected in the *B*-band map, while the extended nature of the H I is evident. At this time, 47 per cent of all gas is beyond the star-forming region. Gas within the star-forming region has average specific angular momentum of $jz_{\rm mean} = 66\,{\rm kpc\,km\,s^{-1}}$ while gas beyond the star-forming region has $jz_{\rm mean} = 131\,{\rm kpc\,km\,s^{-1}}$. Looking at just the H I gas at this time, 20 per cent of H I is beyond the star-forming region, and has $jz_{\rm mean} = 145\,{\rm kpc\,km\,s^{-1}}$. Gas which gains energy directly from supernovae thus has relatively low angular momentum, so simply modelling this gas which is within the star-forming regions as being blown out will preferentially remove low angular momentum material.

4.3 Outflows perpendicular to the disc

Our simulations, as well as observations of outflows, indicate that the situation is more complex than just expelling material from the

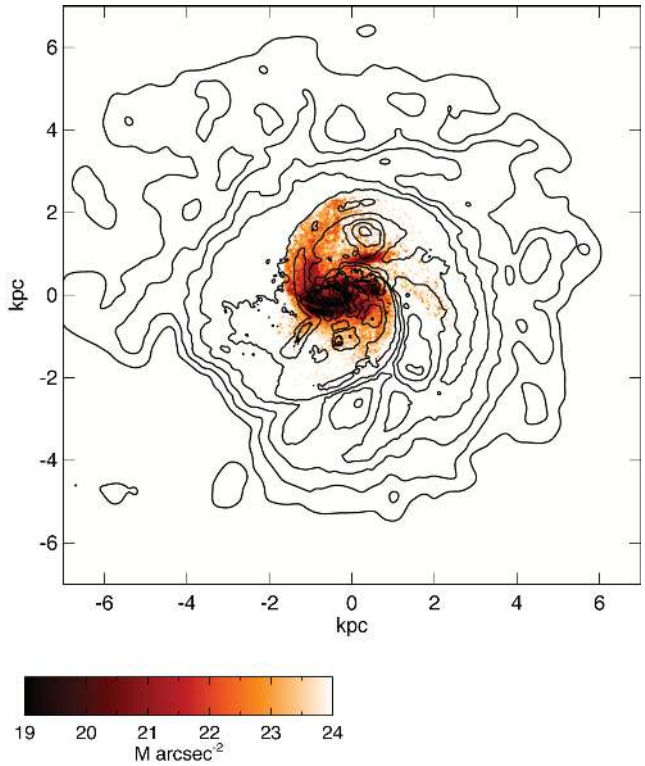

Figure 10. The face-on *B*-band surface brightness map of the galaxy at $z \sim 1.2$, over plotted by an H I contour map. The H I contours range from 10^{19} to 10^{22} cm^{-2} in steps of $10^{0.5}$ cm^{-2}. The extent of the star-forming region is reflected in the *B*-band map, while the extended nature of the H I is evident.

inner, star formation regions of galaxies. As gas is expelled, it can entrain gas which is in outer regions of the galaxy, and sweep it out with the outflows (Stewart et al. 2000; Schwartz & Martin 2004; Veilleux et al. 2005). The relative importance of these two modes of outflow are not well constrained observationally, nor in models. Direct expulsion from inner regions appears to be the dominant mode (Bland-Hawthorn, Veilleux & Cecil 2007), and is the main mechanism in our simulations, although our time resolution makes it difficult to constrain the amount of material which is entrained from the outer regions. But what we can demonstrate is that, consistent with observations (Heckman, Armus & Miley 1987; Bland & Tully 1988; Shopbell & Bland-Hawthorn 1998; Veilleux & Rupke 2002; Bland-Hawthorn, Veilleux & Cecil 2007) and theory (Mac Low & Ferrara 1999; Pieri, Martel & Grenon 2007), the outflows from the central regions are preferentially perpendicular to the plane of the disc.

Fig. 11 shows the direction of gas flows from our galaxy at $z \sim 0.5$, when a minor starburst occurs. The colour gas density map shows the edge on view of the galaxy, with velocity vectors over-plotted showing the direction and magnitude of the gas velocity. The virial radius is marked by a dashed white line. The left-hand panel shows the outflows, and reveals that the outflows follow the path of least resistance perpendicular to the disc. These outflows thus entrain material in regions which are perpendicular to the disc. The highest angular momentum material, which is in the extended gas disc surrounding the star-forming regions, is the least affected by the outflows. We measure a low value for the mean angular momentum in the plane of the disc of this material which is identified as outflows, with $jz_{\rm mean}(\rm outflows) = 20\,kpc\,km\,s^{-1}$, while total angular momentum is high, $j_{\rm mean}(\rm outflows) = 193\,kpc\,km\,s^{-1}$, as the material is getting driven to large radii, perpendicular to the plane, at high velocities. Here, we have used $j_{\rm mean} \equiv \sqrt{jx^2_{\rm mean} + jy^2_{\rm mean} + jz^2_{\rm mean}}$.

By contrast, gas which feeds star formation is forced to fall on the galaxy from a direction which is in the plane of the disc. The right-hand panel of Fig. 11 shows the edge on galaxy, again at $z = 0.5$, but this time only gas which will form stars by $z = 0$ is plotted, again with vectors indicating the velocity of the gas. The gas which feeds star formation is clearly shown to flow primarily from the plane of the disc. This gas has a relatively high planar angular momentum, $jz_{\rm mean}(\rm star\ feed) = 79\,kpc\,km\,s^{-1}$, which is a large fraction of this material's total angular momentum $j_{\rm mean}(\rm star\ feed) = 81\,kpc\,km\,s^{-1}$. This contrasts to the outflowing material, but also to gas which is in the galaxy at this time and which remains in the galaxy as gas at $z = 0$, i.e. material which is neither being ejected nor feeding star formation. Such 'retained' gas

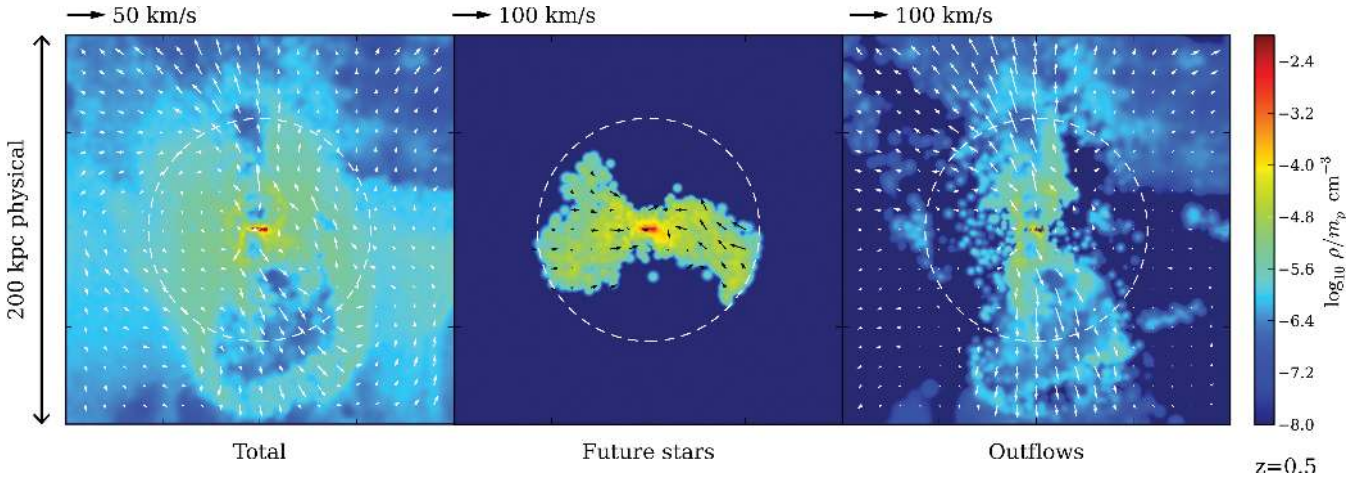

Figure 11. Left-hand panel: the background is a density map of all gases in the simulated galaxy at $z = 0.5$, where the disc is oriented edge on. We have taken a 200 × 200 kpc box. The dashed line marks the virial radius. The arrows are velocity vectors, indicating the direction of outflows, with the size of the arrows related magnitudes of velocities as indicated above the panel. Middle panel: here we plot outflowing gas, again with velocity vectors demonstrating that outflows are strongly directed perpendicular to the disc. Right-hand panel: the gas which is feeding star formation, i.e. we include only gas at $z = 0.5$ which will subsequently form stars by $z = 0$. We use the same scale and again indicate the virial radius. The gas feeding the star formation is accreted largely from low angles from the plane of the disc.

has $jz_{\rm mean}({\rm retain}) = 67\,{\rm kpc\,km\,s^{-1}}$, with total angular momentum, $j_{\rm mean}({\rm retain}) = 127\,{\rm kpc\,km\,s^{-1}}$.

4.4 What about mergers?

One of the characteristic features of CDM cosmology is the mergers of galaxies. This process is ubiquitous, and essentially scale free (e.g. Cole et al. 2000; Fakhouri, Ma & Boylan-Kolchin 2010), meaning that low mass galaxies which become discs will have in general similar merging histories as high-mass galaxies, which have bulges and may be dominated by spheroidal star systems. Mergers are widely expected to result in bulges. In earlier simulations of galaxy formation which suffered from overcooling, protogalaxies rapidly formed dense stellar populations in their central regions. This problem was exacerbated in low-resolution simulations, which have denser central regions (Governato et al. 2008). Loss of angular momentum to dynamical friction in the mergers of such dense protogalaxies resulted in the coalescence of the dense central bulge regions (Navarro & White 1994). The result of the merging of two centrally dense protogalaxies (i.e. those with bulges) were galaxies with large bulges. As explained above, feedback from supernovae prevents a dense bulge forming in the central regions of the protogalaxies in these current simulations. When these protogalaxies which do not have dense central stellar components merge, the most severe effects of dynamical friction are largely mitigated, with gas having been largely 'puffed up' to larger radii, avoiding the cooling catastrophe. Further, as demonstrated in Stewart et al. (2009), direct accretion of stars is insignificant in low-mass galaxies, whose mergers are dominated by gas. The stars which are accreted in the mergers, tend to get thrown into high-energy orbits during the interaction, meaning that the resulting spheroid is not centrally concentrated. A diffuse stellar halo rather than centrally concentrated bulge results from the *scrambled trajectories* of stars during the *late major merger* in our simulation. Indeed, at $z = 0$, our simulated galaxy has an old (mean age 10.3 Gyr), diffuse stellar spheroidal component which comprises $\sim$6 per cent of the stellar mass of the simulated galaxy, even though it has no bulge. This is consistent with observed low mass galaxies in all environments which have old, dim spheroidal stellar populations in addition to their main body of stars (Vansevičius et al. 2004; Hidalgo et al. 2009; Stinson et al. 2009).

Bulges also form during mergers, when gas which was rotationally supported has its orbits scrambled, and cools to the central regions. Hopkins et al. (2009) showed that, when mergers are gas rich, such bulges can be as little as 10 per cent of the resulting galaxy. In such gas rich mergers, no strong bar forms to drive gas to the central regions. Our simulated galaxy has a rich merger history including a merger with mass ratio of 3:1 which has a final coalescence $z \sim 0.8$. All mergers are gas rich, with gas to stellar mass ratio above one for all progenitors of our simulated galaxy. Several reasons ensure that a bulge does not form during these mergers. First, only the inner cold gas is subject to being driven to the centre during the mergers. The surrounding gas is not affected, but we know that inner gas has preferentially low angular momentum. Secondly, in our simulation as in Hopkins et al. (2009), a bar does not form in gas dominated mergers, limiting the amount of gas driven towards the centre.

Thirdly, and most importantly, as gas falls into the dense central regions, feedback prevents large amounts of extended star formation, in a manner similar to what occurs at the centres of early forming protogalaxies in our simulation. The feedback from the small fraction of such gas which forms stars in a burst expels a large fraction of the gas which has lost its angular momentum and has been driven towards the centre of the galaxy, as reflected in the high mass loading during this merging epoch, shown in Fig. 4. Thus, a large fraction of the gas which loses angular momentum and falls to the central regions is expelled. This is clear from the dip in the line traced by squares in Fig. 9, which indicates that the material which loses angular momentum material is removed during the merger. Star formation is primarily occurring in the very inner regions of the merging galaxies, and hence it is the very material that has lost angular momentum which is being blown out. The effective modelling of large scale supernova driven outflows during merger induced star bursts is well supported observationally (Martin 1999; Bland-Hawthorn et al. 2007) and is the extra ingredient in our models which allow us to form bulgeless merger remnants, in contrast to the constrained merger simulations in Hopkins et al. (2009).

5 DISCUSSION

In our simulated dwarf galaxies, we are able to resolve the process of energy injected from multiple overlapping supernovae, which occur in clustered star-forming regions. The thermal energy injected into the surrounding gas creates pressure, and is modelled to undergo a blastwave phase which drives galactic winds. We emphasize that neither degree nor direction of galactic winds are put in by hand within our supernova feedback scheme. Further, it is necessary for the spatial resolution to be significantly less than the scale length of the disc to capture these effects (Colín et al. 2010). More gas is expelled from our simulated galaxies than forms stars by $z = 0$, up to 70 per cent of the original cosmic fraction. Yet, similar to observed isolated dwarfs (Geha et al. 2006), they remain gas dominated at all times, due to the continued cooling of gas into the disc and the low star formation rate. We have previously shown that our model results in simulated dwarf galaxies which match multiple properties of observed dwarf galaxies (Brooks et al. 2011; G10; Oh et al., 2011). Here, we have outlined the reasons that the galactic winds in our simulated galaxies are strongly biased towards expelling low angular momentum gas. We demonstrate the interlinked processes responsible for such bias, which naturally occur when feedback is effectively modelled in a hierarchically assembled galaxy in a CDM Universe.

(i) Low angular momentum material is accreted early. A large fraction of the galaxy's baryonic mass is expelled at these early times.

(ii) A low potential at early times favours early gas ejection.

(iii) Later accreted material has higher angular momentum and forms a disc.

These ideas are similarly outlined by Dekel & Silk (1986) and Binney et al. (2001), where a notion of expelling gas early is invoked to explain the angular momentum of disc galaxies. The high mass loading and high outflow mass to galaxy mass ratio at early times in our simulated galaxy, means that we largely satisfy the Binney et al. (2001) condition of ejecting gas prior to disc formation. Early ejection of material is also postulated in the models of Dutton & van den Bosch (2009) to explain the mass distribution of disc galaxies.

(iv) A reservoir of high angular momentum material exists beyond the star-forming regions.

Disc galaxies have extended H I discs (Broeils & Rhee 1997), as well as warm/hot gas in the halo (Spitzer 1956; Spitzer & Jenkins 1975; Sembach et al. 2003). These act as reservoirs of high angular momentum gas, which are beyond the star formation radius and thus not subject to being directly expelled from the galaxy.

(v) Outflows occur perpendicular to the disc, entraining relatively low angular momentum material and preventing infall of material from regions above and below the disc plane.

Observations strongly indicate that galactic winds expel material perpendicular to galactic discs (Heckman et al. 1987; Shopbell & Bland-Hawthorn 1998; Veilleux & Rupke 2002; Bland-Hawthorn et al. 2007), as predicted by theory (Mac Low & Ferrara 1999; Pieri et al. 2007). Gas which builds the disc at late times is accreted from regions that are relatively aligned to the disc plane.

(vi) Mergers or instabilities which cause gas to lose angular momentum trigger star bursts which expel most of this low angular momentum gas.

Star burst galaxies are generally associated with mergers, and are observed to have significant outflows (Heckman, Armus & Miley 1990; Griffiths et al. 2000; Veilleux et al. 2005) in local galaxies and at high redshift (Pettini et al. 2000; Nestor et al. 2010), predominately driven from the inner starburst regions (Chevalier & Clegg 1985; Strickland & Heckman 2007), ensuring that it is the very material that has lost angular momentum during the merger which is being expelled. High-velocity outflows from post-starburst galaxies are also observed at high redshift (Tremonti, Moustakas & Diamond-Stanic 2007). The high mass loading in these events prevents large amounts of stars being formed from this material which had been driven towards the galaxy's inner regions. Feedback from central black holes/active galactic nuclei (AGN) would also aid in expelling material which has lost angular momentum and has been driven to the central regions. There is evidence to suggest that such feedback is directed perpendicular to the disc (Irwin & Sofue 1992; Su et al. 2010), enhancing the processes outlined in this study.

(vii) A diffuse stellar halo rather than a centrally concentrated bulge results from the scrambled trajectories of stars during the late major merger in our simulation.

The stellar rather than gas component of mergers between progenitors which are massive enough to contain stars themselves, but which do not themselves have bulges, result in a diffuse halo component.

By expelling large amounts of preferentially low angular momentum gas from the galaxy, particularly at early times and during merger events, the shape of the angular momentum distribution of baryons is altered significantly from that of their parent dark matter haloes. This allows the formation of bulgeless disc galaxies. Future work is needed to see if the same processes (possibly in conjunction with black hole/AGN related feedback which also emanates from central regions and thus expels low angular momentum gas) is able to explain the suppression of bulges in more massive halos and the formation of bright disc galaxies with small classical bulges (Kormendy et al. 2010; Peebles & Nusser 2010).

ACKNOWLEDGMENTS

CBB and BKG acknowledge the support of the UK's Science & Technology Facilities Council (STFC Grant ST/F002432/1). CBB and GS thank the DEISA consortium, cofunded through EU FP6 project RI-031513 and the FP7 project RI-222919 for support within the DEISA Extreme Computing Initiative. FG and TQ were supported by NSF ITR grant PHY- 0205413. FG acknowledges support from a Theodore Dunham grant, *HST* GO-1125, NSF grant AST-0607819 and NASA ATP NNX08AG84G. AB acknowledges support from the Sherman Fairchild Foundation. Simulations were run at TACC, ARSC and NAS. We acknowledge the computational support provided by the UK's National Cosmology Supercomputer, COSMOS.

REFERENCES

Adelberger K. L., Shapley A. E., Steidel C. C., Pettini M., Erb D. K., Reddy N. A., 2005, ApJ, 629, 636
Axon D. J., Taylor K., 1978, Nat, 274, 37
Barnes J., Efstathiou G., 1987, ApJ, 319, 575
Barnes J. E., Hernquist L., 1996, ApJ, 471, 115
Binney J., Gerhard O., Silk J., 2001, MNRAS, 321, 471
Bland J., Tully B., 1988, Nat, 334, 43
Bland-Hawthorn J., Veilleux S., Cecil G., 2007, Ap&SS, 311, 87
Booth C. M., Theuns T., Okamoto T., 2007, MNRAS, 376, 1588
Broeils A. H., Rhee M., 1997, A&A, 324, 877
Brooks A. M., Governato F., Booth C. M., Willman B., Gardner J. P., Wadsley J., Stinson G., Quinn T., 2007, ApJ, 655, L17
Brooks A. M., Solomon A., Governato F., McCleary J.Wadsley J., Quinn T., Brook C., 2011, ApJ, 728, 51
Bullock J. S., Kolatt T. S., Sigad Y., Somerville R. S., Kravtsov A. V., Klypin A. A., Primack J. R., Dekel A., 2001, MNRAS, 321, 559
Chevalier R. A., Clegg A. W., 1985, Nat, 317, 44
Cole S., Lacey C. G., Baugh C. M., Frenk C. S., 2000, MNRAS, 319, 168
Colín P., Avila-Reese V., Vázquez-Semadeni E., Valenzuela O., Ceverino D., 2010, ApJ, 713, 535
Daddi E. et al., 2010, ApJ, 713, 686
Dekel A., Silk J., 1986, ApJ, 303, 39
Dutton A. A., 2009, MNRAS, 396, 121
Dutton A. A., van den Bosch F. C., 2009, MNRAS, 396, 141
Fakhouri O., Ma C., Boylan-Kolchin M., 2010, MNRAS, 857
Fall S. M., Efstathiou G., 1980, MNRAS, 193, 189
Geha M., Blanton M. R., Masjedi M., West A. A., 2006, ApJ, 653, 240
Governato F., Willman B., Mayer L., Brooks A., Stinson G., Valenzuela O., Wadsley J., Quinn T., 2007, MNRAS, 374, 1479
Governato F., Mayer L., Brook C., 2008, in Funes J. G., Corsini E. M., eds, ASP Conf. Ser. Vol. 396, The Formation of Galaxy Disks. Astron. Soc. Pac, San Francisco, p. 453 (G10)
Governato F. et al., 2010, Nat, 463, 203
Griffiths R. E., Ptak A., Feigelson E. D., Garmire G., Townsley L., Brandt W. N., Sambruna R., Bregman J. N., 2000, Sci, 290, 1325
Haardt F., Madau P., 1996, ApJ, 461, 20
Heckman T. M., Armus L., Miley G. K., 1987, AJ, 93, 276
Heckman T. M., Armus L., Miley G. K., 1990, ApJS, 74, 833
Hidalgo S. L., Aparicio A., Martínez-Delgado D., Gallart C., 2009, ApJ, 705, 704
Hopkins P. F. et al., 2009, MNRAS, 397, 802
Hopkins P. F. et al., 2010, ApJ, 715, 202
Lynds C. R., Sandage A. R., 1963, ApJ, 137, 1005
McGaugh S. S., 2005, ApJ, 632, 859
Mac Low M., Ferrara A., 1999, ApJ, 513, 142
Madau P., Ferguson H. C., Dickinson M. E., Giavalisco M., Steidel C. C., Fruchter A., 1996, MNRAS, 283, 1388
Maller A. H., Dekel A., 2002, MNRAS, 335, 487
Martin C. L., 1999, ApJ, 513, 156
Martin D. C. et al., 2005, ApJ, 619, L1
Mashchenko S., Couchman H. M. P., Wadsley J., 2006, Nat, 442, 539
Mathews W. G., Baker J. C., 1971, ApJ, 170, 241
Mayer L., Governato F., Kaufmann T., 2008, Adv. Sci. Lett., 1, 7
Navarro J. F., White S. D. M., 1994, MNRAS, 267, 401
Navarro J. F., Frenk C. S., White S. D. M., 1996, ApJ, 462, 563
Navarro J. F., Steinmetz M., 2000, ApJ, 538, 477
Nestor D. B., Johnson B. D., Wild V., Ménard B., Turnshek D. A., Rao S., Pettini M., 2011, MNRAS, 412, 1559
Oh S.-H., Brook C., Governato F., Brinks E., Mayer L., de Blok W. J. G., Brooks A., Walter F., 2011, AJ, submitted
Ohyama Y. et al., 2002, PASJ, 54, 891
Oppenheimer B. D., Davé R., 2006, MNRAS, 373, 1265
Peebles P. J. E., 1969, ApJ, 155, 393

Pettini M., Kellogg M., Steidel C. C., Dickinson M., Adelberger K. L., Giavalisco M., 1998, ApJ, 508, 539
Pettini M., Steidel C. C., Adelberger K. L., Dickinson M., Giavalisco M., 2000, ApJ, 528, 96
Pieri M. M., Martel H., Grenon C., 2007, ApJ, 658, 36
Puech M., Hammer F., Flores H., Delgado-Serrano R., Rodrigues M., Yang Y., 2010, A&A, 510, 68
Quinn T., Binney J., 1992, MNRAS, 255, 729
Robertson B. E., Kravtsov A. V., 2008, ApJ, 680, 1083
Rupke D. S., Veilleux S., Sanders D. B., 2005, ApJS, 160, 115
Ryden B. S., 1988, ApJ, 329, 589
Saitoh T. R., Daisaka H., Kokubo E., Makino J., Okamoto T., Tomisaka K., Wada K., Yoshida N., 2008, PASJ, 60, 667
Sales L. V., Navarro J. F., Schaye J., Dalla Vecchia C., Springel V., Booth C. M., 2010, MNRAS, 409, 1541
Schombert J. M., McGaugh S. S., Eder J. A., 2001, AJ, 121, 2420
Schwartz C. M., Martin C. L., 2004, ApJ, 610, 201
Sembach K. R. et al., 2003, ApJS, 146, 165
Shapley A. E., Steidel C. C., Pettini M., Adelberger K. L., 2003, ApJ, 588, 65
Shopbell P. L., Bland-Hawthorn J., 1998, ApJ, 493, 129
Simcoe R. A., Sargent W. L. W., Rauch M., 2002, ApJ, 578, 737
Spergel D. N. et al., 2003, ApJS, 148, 175
Spitzer L., Jr, 1956, ApJ, 124, 20
Spitzer L., Jr, Jenkins E. B., 1975, ARA&A, 13, 133
Springel V., Hernquist L., 2003, MNRAS, 339, 312
Stewart K. R., Bullock J. S., Wechsler R. H., Maller A. H., 2009, ApJ, 702, 307
Stewart S. G. et al., 2000, ApJ, 529, 201
Stinson G., Seth A., Katz N., Wadsley J., Governato F., Quinn T., 2006, MNRAS, 373, 1074
Stinson G. S., Dalcanton J. J., Quinn T., Gogarten S. M., Kaufmann T., Wadsley J., 2009, MNRAS, 395, 1455
Strickland D. K., Heckman T. M., 2007, ApJ, 658, 258
Tasker E. J., Bryan G. L., 2008, ApJ, 673, 810
Teyssier R., Chapon D., Bournaud F., 2010, ApJ, 720, 149
Thacker R. J., Couchman H. M. P., 2000, ApJ, 545, 728
Tremonti C. A., Moustakas J., Diamond-Stanic A. M., 2007, ApJ, 663, L77
van den Bosch F. C., 2001, MNRAS, 327, 1334
van den Bosch F. C., Burkert A., Swaters R. A., 2001, MNRAS, 326, 1205
Vansevičius V. et al., 2004, ApJ, 611, L93
Veilleux S., Rupke D. S., 2002, ApJ, 565, L63
Veilleux S., Cecil G., Bland-Hawthorn J., 2005, ARA&A, 43, 769
Verde L. et al., 2003, ApJS, 148, 195
Wadsley J. W., Stadel J., Quinn T., 2004, New Astron., 9, 137

This paper has been typeset from a TEX/LATEX file prepared by the author.